



# Quantifying time lag of epikarst-spring hydrograph response to rainfall using correlation and spectral analyses

Zhicai Zhang · Xi Chen · Xunhong Chen · Peng Shi

**Abstract** Understanding spring-flow characteristics in karst areas is very important for efficient utilization of water resources. The time lag of a spring-hydrograph response to rainfall is related to karst hydrogeological properties such as thickness, porosity and hydraulic conductivity. The length of the time lag can be determined based on results of the time-series analysis. However, some approaches, with different identifying indicators, give different lengths of the time lag. In this study, the flow-discharge series of two hillslope springs located in a karst area of southwest China were used to compute lengths of the time lag. The thickness and porosity of the epikarst-zone fractures on the two hillslopes were estimated based on a ground-penetrating radar investigation and field measurement. Based on comparison of lengths of the time lag computed by auto- and cross-correlation analyses, the identifying indicators of the time lag were classified into three types for measuring short, intermediate and long-term responses of the spring hydrograph to rainfall. The study also reveals that the time lag of spring-hydrograph response to rainfall in the thick epikarst zone is much longer than that in the thin epikarst zone.

**Keywords** Epikarst · Spring discharge · Time lag · Time series analysis · China

## Introduction

The epikarst zone is located at the top of the aerated or vadose zone in carbonate rocks (Mangin 1975; Williams 1983). Epikarst near the ground surface has a large permeability, offering fast water infiltration. As the extent and frequency of fractures diminish gradually with depth, epikarst permeability also diminishes with depth (Ford and Williams 2007). Consequently, after recharge, percolating rainwater is retained near the base of the epikarst leading to the formation of an epikarstic aquifer (Williams 2008). Part of the stored water percolates downwards through the transmission zone to the saturated zone, and the remaining water emerges on the hillslope's lower area as an epikarst spring. Spring discharge from the epikarst zone is an important groundwater resource in karst areas. It is commonly used for irrigation in the hilly mountainous areas in the southwest karst region of China. Characteristics of spring discharge variations associated with climate fluctuation, particularly with climatic extremes, are very important for social and economic development. For example, the extremely severe drought in the southwest provinces of China in 2010 affected 80,700 ha of farmland, leading to a shortage of drinking water for about 26 million people due to dry-up of springs in the mountain areas.

The epikarst spring hydrograph is derived from a response to diffuse recharge over the entire epikarst network. The capacity to absorb, store and transmit precipitation of the epikarst zone strongly influences the epikarst spring hydrograph. Variations of the spring discharge depend on epikarst thickness, porosity and hydraulic conductivity. Well-developed karstic features result in significant attenuation of the input signal of precipitation due to the effect of a thick non-saturated zone (Benavente et al. 1985). The epikarst distributes infiltrated water as either a base flow component (flowing in mini fracture and matrix) or a quick flow component (flowing in wide fracture or conduit; Perrin 2003). In the case of a small storage volume of aquifer, most of the water is retained and stored in the base of the epikarst zone, and this water slowly seeps through tiny fractured rock blocks and diffusely recharges the lower parts of an aquifer (Trček 2007).

The storage capacity of a karst aquifer and its effect on rainfall-flow-discharge response can be described by

---

Received: 17 December 2012 / Accepted: 20 August 2013  
Published online: 11 September 2013

© Springer-Verlag Berlin Heidelberg 2013

---

Z. Zhang · X. Chen · P. Shi  
State Key Laboratory of Hydrology-Water Resources and Hydraulic Engineering,  
Hohai University, Nanjing, 210098, China

Z. Zhang · X. Chen (✉) · P. Shi  
College of Hydrology and Water Resources,  
Hohai University, Nanjing, 210098, China  
e-mail: xichen@hhu.edu.cn

X. Chen  
School of Natural Resources,  
University of Nebraska-Lincoln, Lincoln, NE, USA

memory effect and regulation time of a karst system. The memory effect proposed by Mangin (1984) reflects the inertia of the system. It determines the impulse response or the length of time the input signal persists in the system. The regulation time is another measure of memory effect of the system, but it is less sensitive to the sampling interval and correlation between distant events than the memory effect. It is considered that a high memory effect is often related to a large storage capacity of the system (Mangin 1984). A well-developed karst aquifer with larger conduits and without a significant water-storage capacity should correspond to a low memory and short response-time system (Larocque et al. 1998; Panagopoulos and Lambrakis 2006). That is the main reason why streamflow hydrographs for karst regions present a steep rise and decline in areas that are rich in rock fractures and underground conduit systems (Chen et al. 2008).

Time series (Box et al. 1994) are useful to identify the memory effect and regulation time, and to establish the way in which the system modulates the input signals of rainfall events (Benavente et al. 1985). Correlation and spectral analyses are forms of time-series analysis which are usually easy to implement based on a system approach as they relate input signals (rainfall) to output signals (hydrograph) through the use of statistical functions. In a karst aquifer, analysis of time lag between input and output signals can be based on the individual signal of a spring hydrograph which provides an integrated representation of the network of stores and passages delivering water to the aquifer outflow point (Ford and Williams 1989; Bonacci 1993). Another analysis of the time lag is to compare input and output signals. The aquifer is considered as a filter which transforms, retains, or eliminates the input signal in the creation of an output signal. The degree of transformation of the input signal therefore provides valuable information on the nature of flow in the system.

Different approaches of correlation and spectral analyses may give different lengths of the time lag. One approach is based on the shape of a correlogram (discharge-discharge) of the autocorrelation function and spectral density function. Lengths of the time lag are identified by different indicators. The correlogram stresses the linear dependence of successive events for increasing time intervals. The events can be considered quasi-independent and the correlogram value is essentially identical to the autocorrelation of noise when the correlogram value is below threshold value such as 0.2 (Amraoui et al. 2003; Mangin 1984). Mangin (1984) proposed that the time required for the correlogram to drop below the threshold value is treated as the memory effect. The spectral analysis corresponds to a change from a time domain to a frequency domain through a Fourier transform of the correlogram. The simple spectral density function also enables the regulation time of the system to be calculated.

Another approach is based on a cross-correlogram (rainfall-discharge) of the cross-correlation function and cross-spectral density function. It estimates a time lag of

the cross-correlation between input (rainfall) and output (hydrograph), indicating an estimation of the pressure pulse transfer times through the aquifer (Panagopoulos and Lambrakis 2006). The cross-spectral density function is used complementarily to the cross-correlation analysis in order to calculate the mean delay, concerning different frequencies between precipitation and spring discharge (Padilla and Pulido-Bosch 1995; Larocque et al. 1998). The cross-correlation and cross-spectral density function give an idea about the impulsive response of the karst system, as well as about the quality of drainage and the groundwater flow reserves of the aquifer. They can be used for identifying the duration of the impulse response of the aquifer's baseflow component and the duration of the quickflow component (Padilla and Pulido-Bosch 1995). The time shift between signal input and output was used for estimating conduit flow transit times (Maloszewski et al. 2002).

As a useful method in karst hydrology research, time-series analysis was used when the karst aquifer is considered as a black box. However, the analysis results by different methods give various lengths of the time lag between input and output. Explanation of the results from the time-series analysis requires information of an aquifer and its influence on flow processes in a karst system (Eisenlohr et al. 1997). In this study, observation stations at two study sites were set up for collecting precipitation and karst spring discharge. The epikarst structure of the two study sites was investigated by ground-penetrating radar (GPR). The different hydrograph behaviors of the two sites, shown by the results of the time-series analysis, are interpreted as associated with the epikarst structures of the two sites. The lengths of the time lags computed by different approaches of auto- and cross-correlation analyses were used as identifying indicators of response of the flow in the karst system to rainfall. The identifying indicators were classified into three types for measuring short, intermediate and long-term responses of spring hydrographs to rainfall.

## Description of field site and spring flow observation

The overall study site is spread over adjacent mountains in a small karst basin of Chenqi at the Puding Karst Ecohydrological Observation Station, Guizhou Province of southwest China (Fig. 1). The southwest karst area, located on the Yunnan-Guizhou Plateau, is one of the largest, continuous karst areas in the world. Carbonate rock is widespread and accounts for 62 % of the total land area. The site has a subtropical wet monsoon climate with mean annual temperature of 20.1 °C, highest in July and lowest in January. Annual precipitation is 1,140 mm, with a distinct wet summer season from May to September and a dry winter season from October to April. Average monthly humidity ranges from 74 to 78 %. The karst in south Guizhou is developed mainly in the Carboniferous-Permian limestones or in the Middle-Lower Triassic

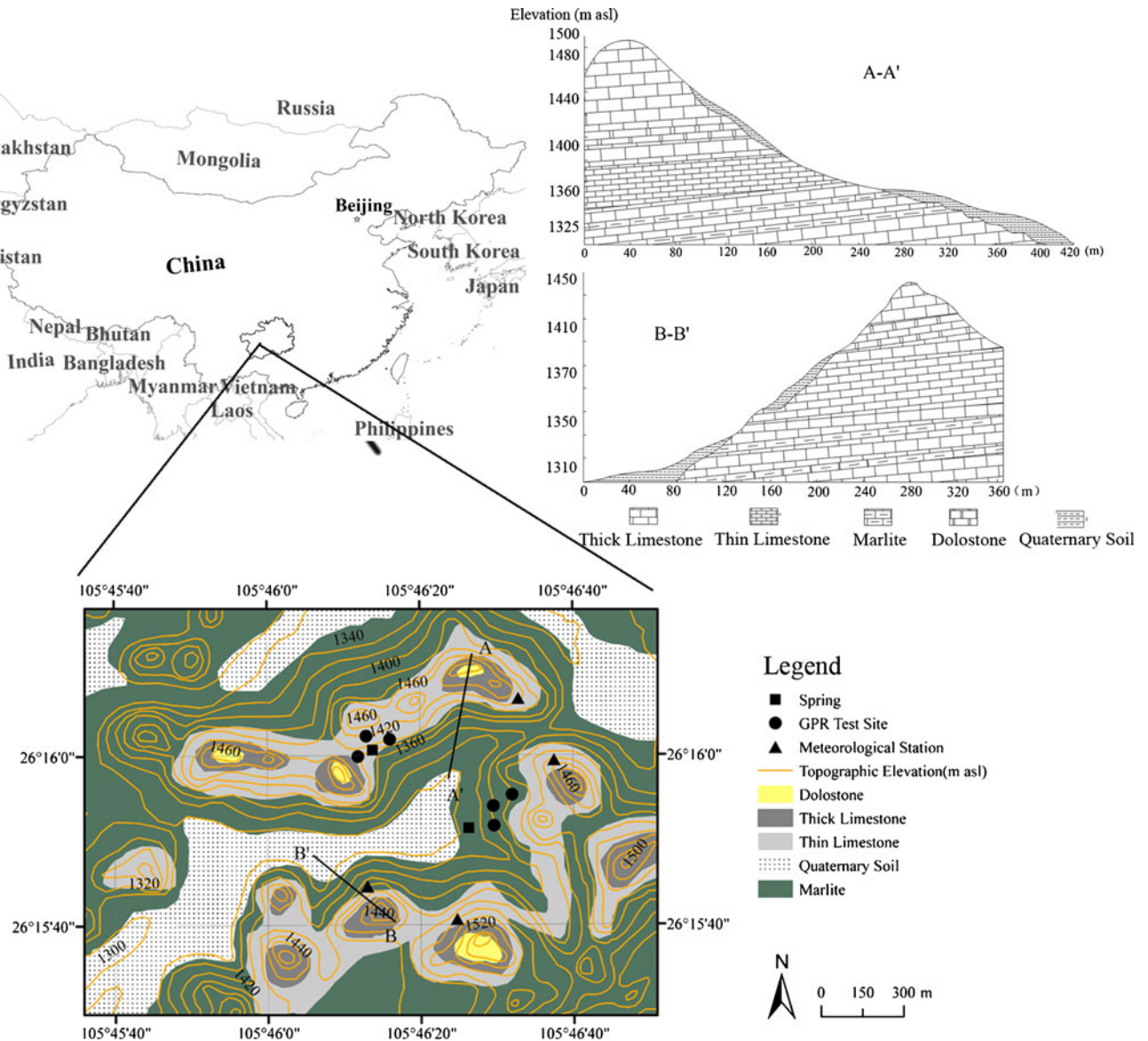


Fig. 1 Hydrogeological map of the study site

limestones and syngenetic dolomite. Geological strata in the study basin include dolostone, thick and thin limestone, marlite and Quaternary soil. Limestone formations with 150–200 m thickness lie above an impervious marlite formation. The Quaternary soils developed on carbonate rocks are very thin, and the average soil thickness is about 50 cm. Some limestone fragments are mixed in with the soils, and the rock outcrop area is 10–30 %. The vegetation species include deciduous broad-leaved forest at the top and middle of the mountain and crops on the lower part of the mountain.

The two selected epikarst springs, ZJS and ELP, are located on the upper hillslope of Zhangjiashan mountain (ZJS) and the lower hillslope of Erlapo mountain (ELP) (Fig. 1). The hourly precipitation was measured using HOBO automatic meteorological equipment in this basin. The hourly spring flow discharges at the two outlets of the ZJS and ELP hillslopes were estimated by triangular notch

weirs, at which water level was automatically measured by HOBO U20 water level loggers.

### Methods of time-series analysis and GPR investigation

Time-series analysis can be used to compare entry signals (rainfall) and output signals (hydrograph). The information of the signals can be treated individually (auto-correlation analysis) or by comparison to one another (cross-correlation analysis). The functions of time-series analysis include autocorrelation, univariate spectral density, cross-correlation, cross-amplitude, gain, coherency and phase functions. For more detailed explanations and the complete theoretical development refer to Jenkins and Watts (1968), Mangin (1984), Box et al. (1994), Padilla and Pulido-Bosch (1995) and Larocque et al. (1998).

**Autocorrelation and spectral analysis**

Autocorrelation and spectral analysis characterize the individual structure of time series: autocorrelation in the time domain, and spectral density in the frequency domain. The autocorrelation function,  $r(k)$ , is a normalized measure of the linear dependence of successive values over a time period (Larocque et al. 1998; Lambrakis et al. 2000) :

$$r(k) = \frac{C(k)}{C(0)} \tag{1}$$

where  $C(k)$  is the correlogram, reflecting the memory of the system:

$$C(k) = \frac{1}{n} \sum_{t=1}^{n-k} (x_t - \bar{x})(x_{t+k} - \bar{x}) \tag{2}$$

$$C(0) = \frac{1}{n} \sum_{t=1}^n (x_t - \bar{x})^2 \tag{3}$$

where  $k$  is the time lag ( $k=0$  to  $m$ ),  $n$  is the length of the time series,  $t$  is time,  $x$  is a single event measurement,  $\bar{x}$  is the mean of the event measurements and  $m$  is the cutting point. The cutting point determines the interval in which the analysis is carried out. The plot of the autocorrelation function as a function of lag is also called the correlogram.

To determine whether the autocorrelation at lag  $k$  is significantly different from zero, the following hypothesis and rule of thumb may be used. For any  $k$ , reject  $H_0$  if

$$|r_k| > \frac{2}{\sqrt{n}} \tag{4}$$

where  $n$  is the number of observations, and this rule of thumb is for  $\alpha=5\%$  in this study.

The autocorrelation function  $r(k)$  also determines how the variance of the series considered is distributed over the different frequencies (Gand et al. 1991). According to the Fourier's transformation of autocorrelation function  $r(k)$ , univariate spectral analysis can be used to change from a time mode to a frequency mode  $S(f)$ :

$$S(f) = 2 \left[ 1 + 2 \sum_{k=1}^m D(k)r(k) \cos(2\pi fk) \right] \tag{5}$$

$$D(k) = \frac{1 + \cos \pi \frac{k}{m}}{2} \tag{6}$$

where  $f$  is the frequency and  $D(k)$  ensures that the  $S(f)$  estimated values are not biased.

The spectral density function determines the regulation time,  $T_{reg}$ , defined as half of the maximum spectral intensity as the frequency  $f$  goes to zero and the period goes toward infinity:

$$T_{reg} = \frac{S(f=0)}{2} \tag{7}$$

The regulation time,  $T_{reg}$ , defines the duration of the influence of the input signal and gives an indication of the length of the impulse response of the system (Larocque et al. 1998; Lee and Lee 2000).

**Cross-correlation and cross-spectral analysis**

The cross-correlation and cross-spectral analysis considers transformation of the input to the output signal, such as rainfall and outlet spring discharge of a watershed. The cross-correlation function,  $r_{xy}(k)$ , represents the interrelationship between the input and output series (Lee and Lee 2000), and it is analyzed in a time domain:

$$r_{xy}(k) = \frac{C_{xy}(k)}{\sqrt{C_x^2(0)C_y^2(0)}} \tag{8}$$

$$C_{xy}(k) = \frac{1}{n} \sum_{t=1}^{n-k} (x_t - \bar{x})(y_{t+k} - \bar{y}) \tag{9}$$

$$C_x(0) = \frac{1}{n} \sum_{t=1}^n (x_t - \bar{x})^2 \tag{10}$$

$$C_y(0) = \frac{1}{n} \sum_{t=1}^n (y_t - \bar{y})^2 \tag{11}$$

where  $C_{xy}(k)$  is the cross-correlogram. Time of correlogram peak can be estimated as the lag at which the estimated cross correlation between input and output is maximal.

The cross-spectral density function,  $S_{xy}(f)$ , corresponds to the Fourier transform of the cross-correlation function. It is expressed as a function of the cospectrum,  $h_{xy}(f)$ , and the quadrature spectrum,  $\lambda_{xy}(f)$ .

$$S_{xy}(f) = h_{xy}(f) - i\lambda_{xy}(f) \tag{12}$$

$$h_{xy}(f) = 2 \left\{ r_{xy}(0) + \sum_1^m [r_{xy}(k) + r_{yx}(k)] D(k) \cos(2\pi fk) \right\} \tag{13}$$

$$\lambda_{xy}(f) = 2 \left\{ \sum_1^m [r_{xy}(k) - r_{yx}(k)] D(k) \sin(2\pi fk) \right\} \tag{14}$$

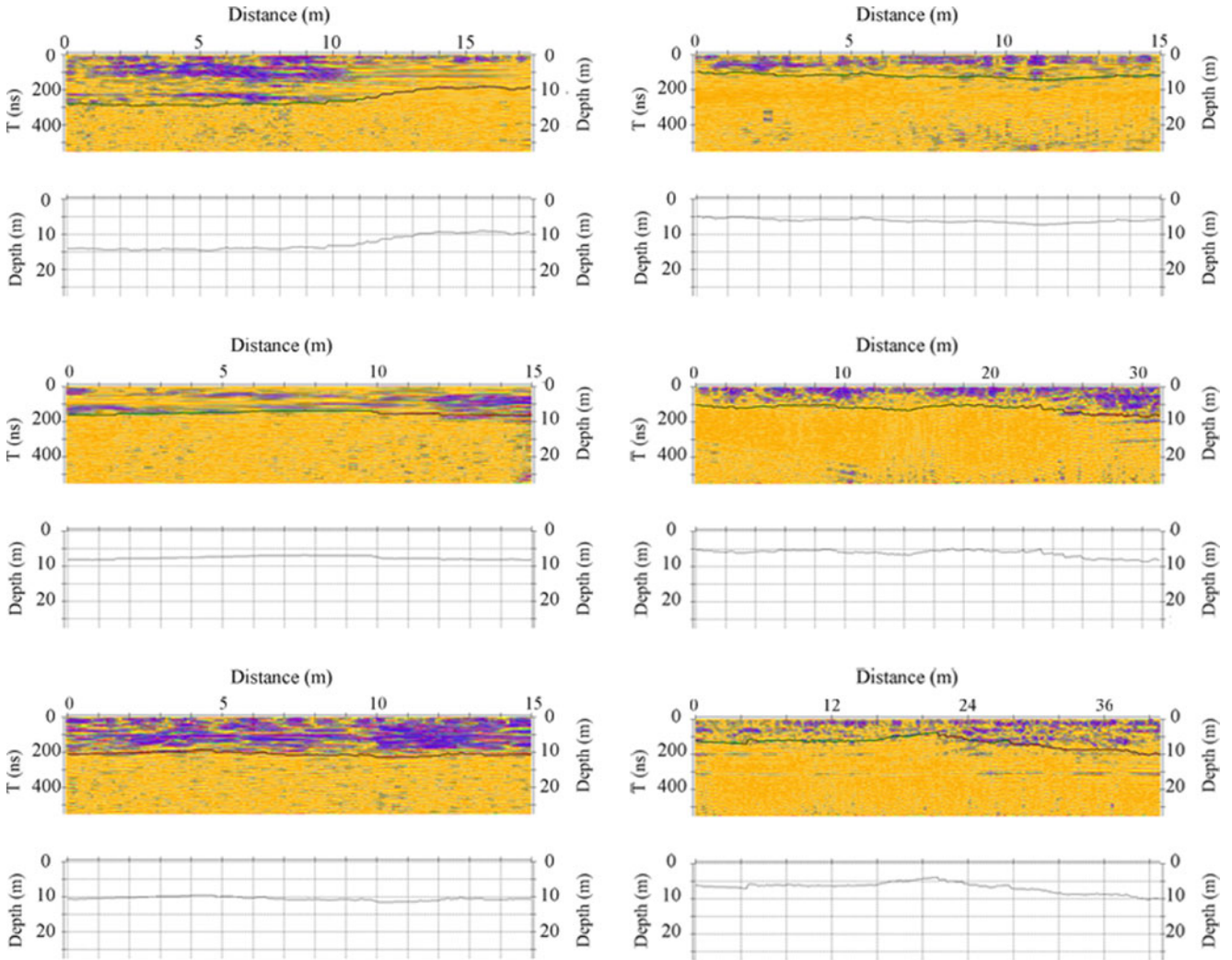


**Fig. 2** GPR observations of the epikarst zone for ZJS hillslope (Z1, Z2 and Z3) and ELP hillslope (E1, E2 and E3). The *top* profile represents the radargramme reflex of the GPR transect; the *bottom* profile represents the depth transformed by picked traveltimes of the reflectors using mean velocity of electromagnetic waves ( $0.1 \text{ m ns}^{-1}$ ); the *solid line* in the profile represents the base of the epikarst

where  $r_{xy}(k)$  and  $r_{yx}(k)$  are the cross-correlation coefficients, and  $D(k)$  is determined using Eq. (6).  $r_{xy}(k)$  can be determined by the similar equation as Eq. (8).

$$r_{yx}(k) = \frac{C_{yx}(k)}{\sqrt{C_x^2(0)C_y^2(0)}} \quad (15)$$

$$C_{yx}(k) = \frac{1}{n} \sum_{t=1}^{n-k} (y_t - \bar{y})(x_{t+k} - \bar{x}) \quad (16)$$

In polar coordinates, the cross-spectrum  $S_{xy}(f)$  can also be expressed as a function of the amplitude,  $|S_{xy}(f)|$ , and phase,  $\theta_{xy}(f)$ :

$$S_{xy}(f) = |S_{xy}(f)|e^{-i\theta_{xy}(f)} \quad (17)$$

$$|S_{xy}(f)| = \sqrt{h_{xy}^2(f) + \lambda_{xy}^2(f)} \quad (18)$$

$$\theta_{xy}(f) = \arctan \frac{\lambda_{xy}(f)}{h_{xy}(f)} \quad (19)$$

In the karst area with a predominant role of the fast-flow component and relatively small regulation effect, the cross-spectrum usually shows small altering of the input signals, and high values at low frequencies. Hence, the time corresponding to the frequency that the cross-spectrum  $S_{xy}(f)$  tends to zero, can be used to quantify short term response of the spring hydrograph to rainfall for a highly developed karst hydrogeological system. The phase function  $\theta_{xy}(f)$  can be used complementary to the cross-correlation analysis in order to calculate the mean delay for different frequencies between rainfall and spring discharge (Padilla and Pulido-Bosch 1995; Larocque et al.

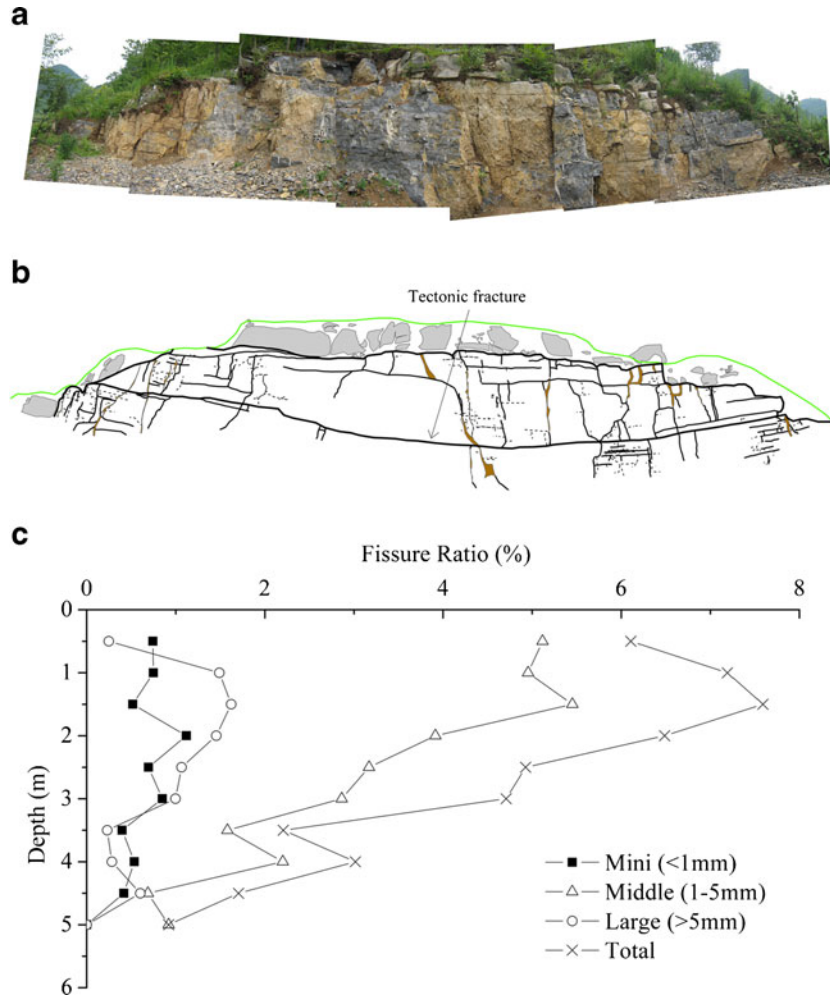


**Fig. 3** A fracture profile in the study site: **a** photograph of an outcrop, **b** digitized profile of the fracture network shown in the photograph (a), and **c** vertical distribution of fracture ratio

1998). From Eq. (17), the time delay  $d$  appears in the cross-spectrum as a phase function  $\theta_{xy}(f)=2\pi fd$ . The delay  $d$  is

$$d = \frac{\theta_{xy}(f)}{2\pi f} \tag{20}$$

The coherency function,  $CO_{xy}(f)$  is:

$$CO_{xy}(f) = \frac{S_{xy}(f)}{\sqrt{S_x(f)S_y(f)}} \tag{21}$$

where  $S_x(f)$  and  $S_y(f)$  are the spectral-density functions of the series  $x$  and  $y$ , respectively.

The coherency function expresses the linearity of the karst system (Larocque et al. 1998). The linearity is a characteristic of a highly karstified aquifer, where a heavy rainfall event produces a strong discharge of the karst spring over a short period of time.

The gain function,  $g_{xy}(f)$ , expresses the amplification ( $>1$ ) or attenuation ( $<1$ ) of the output data in relation to the input signal (Larocque et al. 1998):

$$g_{xy}(f) = \frac{S_{xy}(f)}{S_x(f)} \tag{22}$$

**Table 1** Statistical results of fractures for the profile shown in Fig. 3

Fracture types	Whole section		Upper section		Lower section	
	Fracture area (cm <sup>2</sup> )	Porosity (%)	Fracture area (cm <sup>2</sup> )	Porosity (%)	Fracture area (cm <sup>2</sup> )	Porosity (%)
Mini	5,662.7	0.7	3,521.3	0.8	2,141.4	0.5
Middle	27,170.4	3.1	20,405.5	4.6	6,764.9	1.7
Large	12,673.9	1.5	7,018.0	1.6	840.0	0.2
Total	45,507.0	5.3	30,944.8	6.9	9,746.3	2.4
Section area	855,325.8	–	448,913.2	–	406,412.6	–

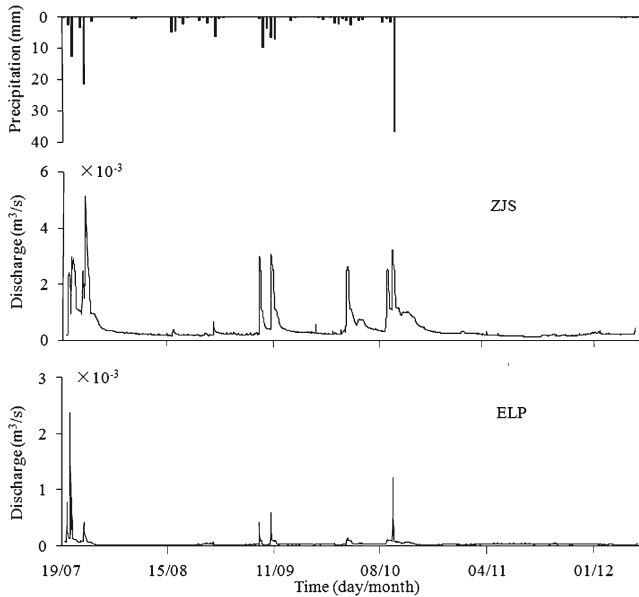


**Fig. 4** Hydrographs of *ZJS* and *ELP* springs during the study period in 2010

### GPR investigation

GPR is a high-resolution geophysical technique that utilizes the transmission and reflection of high frequency (10–1,200 MHz) electromagnetic waves. This method appears particularly well for analysis of the near-surface (<30 m in depth) structure of a karst zone, especially when clayey coating or soil that absorbs and attenuates the radar is rare and discontinuous. For hydrogeology, GPR is applied to locate fractured or karstified zones, faults and cavities in terms of changes in electromagnetic properties (Beres and Haeni 1991; McMechan et al. 1998; Beres et al. 2001; Al-fares et al. 2002). In this study, a GPR MALA Professional Explorer (ProEx) System was used for investigation of the epikarst thickness on the sites with a RTA 50-MHz antenna frequency. It is composed of a control unit (ProEx), connected to a portable computer for the direct recording of raw data. The ProEx itself is connected to the radiating-receiving antennae via optical fibers. For limestone, the average velocity of electromagnetic waves is 0.1 m/ns (Al-fares et al. 2002). It is the value used for most of the profiles carried out in reflection mode in the karst area. According to the average velocity

and the corresponding time window, the depth of an object can be calculated. REFLEX 2D (Sandmeier geophysical software) was used for processing of GPR data.

## Results

### Investigation of epikarst structures

Six parallel profiles within the flow concentration area of Zhangjiashan (*ZJS*) and Erlapo (*ELP*) springs were investigated using the GPR technique on the two hillslopes (Fig. 1). Three profiles (*Z1*, *Z2* and *Z3*) were located at lower areas of *ZJS* hillslope while the other three profiles (*E1*, *E2* and *E3*) were located at upper areas of *ELP* hillslope (Fig. 1). The GPR sites selected in this study are located in the flow concentration area of the two springs. In order to make investigation sites representative, the sites with different elevation, orientation and microtopography were chosen for each hillslope (Fig. 1). Therefore, the GPR sites selected are representative for study of epikarst thickness in hillslopes. The radargrammes clearly show several structures that characterize the karstic aquifer near the surface. The purple color in the upper profiles in Fig. 2 represents the low propagation velocity of electromagnetic wave in the ground. The zone with intensive changes of color is characterized by strong fractured rocks. Relatively, the yellow color at the bottom indicates high-propagation velocity of the electromagnetic wave and represents the less-weathered limestone.

The epikarst thickness at three locations on *ZJS* hillslope (*Z1*, *Z2* and *Z3* in Fig. 1) and the other three locations on *ELP* hillslope (*E1*, *E2* and *E3* in Fig. 1) were estimated. Along investigation profiles, the soil cover is very thin, 30–60 cm for *Z1*–*Z3* and 0–50 cm for *E1*–*E3*. The results in Fig. 2 show that the mean epikarst depth is 12.56, 7.6 and 10.36 m along profiles of *Z1*, *Z2* and *Z3*, respectively. The mean epikarst depth is 6.05, 6.16 and 6.74 m along *E1*, *E2* and *E3*, respectively. This reveals that the epikarst zone at the lower areas of hillslope *ZJS* (*Z1*–*Z3*) is greatly deeper than that at the upper areas (*E1*–*E3*; Zhang et al. 2011).

Fracture apertures and lengths were measured in an exposure profile within this basin (Fig. 3(a)). There is a tectonic fracture system of about 5 m beneath the land surface in this profile. The fracture apertures were classified into three types according to aperture width:

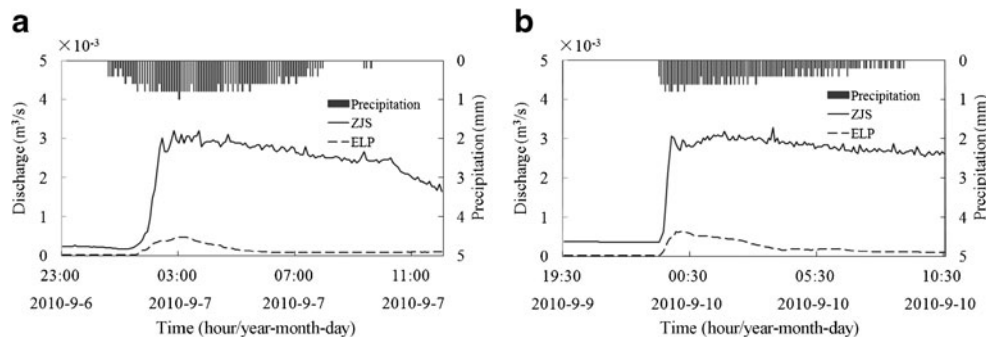


**Fig. 5** Two representative hydrographs of *ZJS* and *ELP* springs on **a** September 7 and **b** September 9–10, 2010

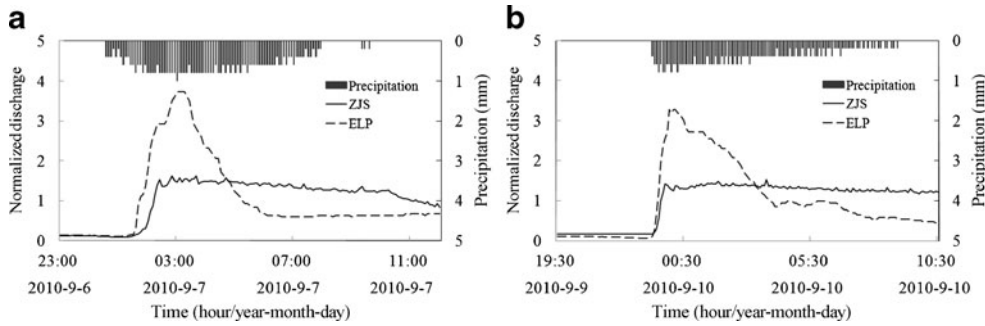


**Fig. 6** Normalized flow discharges for the two representative hydrographs of ZJS and ELP springs on **a** September 7 and **b** September 9–10, 2010

mini fracture with aperture less than 1 mm, middle fracture with aperture between 1 and 5 mm, and large fracture with aperture larger than 5 mm. The fracture porosity was estimated by fracture area (fracture aperture multiplies length) divided by the section area.

The statistical results show that total porosity of this section is 5.3 %, consisting of porosity of 0.7 % for the mini fractures, 3.1 % for the middle fractures and 1.5 % for the large fractures (Table 1). The porosity is 6.9 % for the upper section (above the tectonic fracture), and 2.4 % for the lower section (under the tectonic fracture). Further analysis, by dividing the section into 10 layers with an interval of 0.5 m in thickness, shows that the porosity decreases with the increase of depth from the ground surface (Fig. 3c). The porosity decreases from 6.1 % in the uppermost layer to 0.9 % in the lowest layer at 5 m depth from ground surface.

**Response of spring flow to two rainfall events**

The hourly precipitation and flow discharge series from July 19 to December 11, 2010 for the ZJS and ELP springs were used for this study (Fig. 4). The total length of the time series is 6 months and each data set consists of 3,470 readings.

During the study period, the following two flood events were selected as an example to show different characteristics of rainfall-flow-discharge response for the two springs: one event occurring from (times) 00:00 to 08:00 on September 7, 2010, and the other from 23:00 on September 9 to 09:00 on September 10, 2010 (Fig. 5). The rainfall amount was 55.2 mm for the flood event on

September 7, and 45.2 mm for the flood event during September 9–10. The first flood started from an initially dry condition with a consecutive no-rainfall period of 11 days from August 27 to September 6. In contrast, the initial condition of the second flood was relatively wet.

For the two flood events during the period of September 7~10, mean flow discharge for ZJS spring was  $2 \times 10^{-3} \text{ m}^3/\text{s}$ , much greater than  $1 \times 10^{-4} \text{ m}^3/\text{s}$  for ELP spring (Fig. 5). A measure of the ‘flashiness’ of the response is given by the normalized spring discharge in terms of the ratio of discharge,  $q_t$ , to its mean value,  $\bar{q}$  ( $q_t/\bar{q}$ ), for individual storms. Temporal variations of flow discharges of these two springs can be clearly seen from the normalized spring discharges in Fig. 6. The normalized hydrograph of ELP spring changes more dramatically than that of ZJS spring (Fig. 6). After the peak flood, decrease in the flood discharge for ELP spring is more rapid than that for ZJS spring. The slow recession for ZJS spring implies that the thick epikarst zone of ZJS hillslope has great regulation capacity.

Moreover, rising of the normalized flow discharge responding to rainfall is closely related with initially dry and wet conditions of the epikarst zone. For the flood event with an initially dry condition on September 7, 2010, the time lag between rainfall and flow occurrence was 1 h and 50 min for ZJS and ELP hillslopes, respectively. Comparatively, for the flood event with an initially wet condition on September 10, 2010, the time lag was reduced to 10 and 5 min for ZJS and ELP, respectively. Flood flow started as rainfall amount was accumulated to about 5 mm for the initially dry condition and only 1 mm for the initially wet conditions.

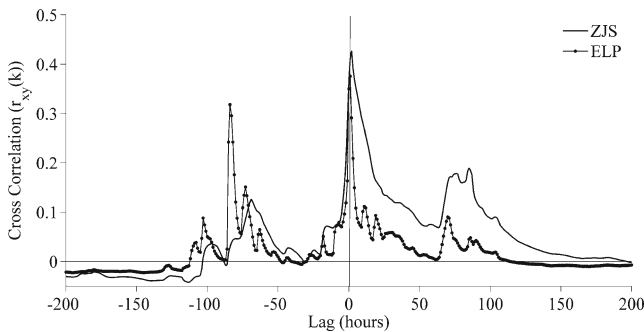


**Fig. 7** Cross-correlation functions of flow discharges for ZJS and ELP springs

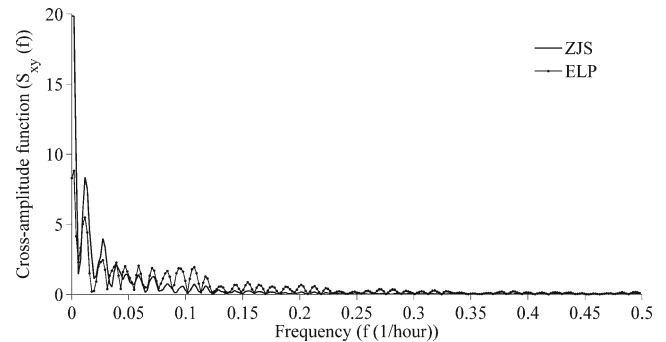


**Fig. 8** Cross-amplitude functions of flow discharges for ZJS and ELP springs



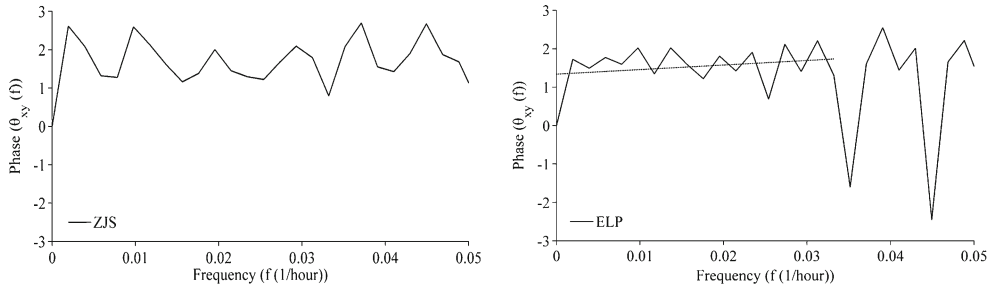


**Fig. 9** Phase functions of flow discharges for ZJS and ELP springs

**Results of time-series analysis**

The functions of time-series analysis including autocorrelation, spectral density, cross-correlation, cross-amplitude, gain, coherency and phase functions were computed using the hourly precipitation and discharge data of the ZJS and ELP springs from July 19 to December 11, 2010. They are shown in Figs. 7, 8, 9, 10, 11, 12, and 13. Lengths of the time lag derived from these figures are listed in the Table 2. Due to the strong heterogeneity of the karst fracture system, flow in the solution conduit is much faster than that in the surrounding carbonate rocks (matrix). Thus, the lengths of the lag time for the mixed flow karst systems can be classified as three types. The first type refers to short-term response of spring hydrograph to rainfall, indicating fast response of the flow from large fractures and conduits to the heavy rainfall events. It can be analyzed by the cross correlation between input and output and interpreted by indicators of the time of correlogram  $r_{xy}(k)$  peak, the delay time of  $d = \frac{\theta_{xy}(f)}{2\pi f}$ , and the time corresponding to the frequency that the cross-spectrum  $S_{xy}(f)$  tends to zero. The second type refers to long-term response of spring hydrograph to rainfall as recession of groundwater flow from the small fractures becomes much slower after a long nonrainfall period or the impulse response of the groundwater flow to a short-term rainfall becomes insignificant. It can be quantified by indicators of the memory effect and the regulation time using auto-correction analysis to indicate the slow recession of spring flow, and the lengths between periodic intervals of auto- and cross-correlograms to indicate long-term response of spring flow to rainfall events. The third type refers to intermediate term response of spring hydrograph to rainfall as the impulse response of the karst

system to the input signature varies from significant to insignificant. It can be quantified by indicators of the duration of the sharp decline of auto- and cross-correlograms.

*Short-term response of spring hydrograph to rainfall*

Results in Table 2 show that the short term response is computed by the cross-correlation, cross-amplitude and phase function. The cross-correlation function ( $r_{xy}(k)$  in Fig. 7) shows a clear dissymmetry towards the positive  $k$  values, indicating that the rainfall influences the flow rates of the spring. The delay, which is the time lag between  $k=0$  and the maximum  $r_{xy}(k)$ , determines the stress transfer velocity of the system. The correlogram shows the strongest cross-correlation for a time lag of 2 h ( $r_{xy}(2\text{ h})=0.43$ ) for ZJS spring and a time lag of 1 h ( $r_{xy}(1\text{ h})=0.38$ ) for ELP spring.

The cross-amplitude function of ELP and ZJS springs ( $|S_{xy}(f)|$  in Fig. 8) shows small altering of the input signals, and high values at low frequencies.  $|S_{xy}(f)|$  decreases slowly at middle and high frequencies and tend to zero for frequencies above  $0.35\text{ h}^{-1}$  (periods of less than 3 h) and  $0.2\text{ h}^{-1}$  (periods of less than 5 h) for the ELP and ZJS springs, respectively.

The phase function ( $\theta_{xy}(f)$  in Fig. 9) indicates the mean delay between rainfall and flow discharge. The phase function of the ELP spring shows alignment only for the frequencies between 0 and  $0.033\text{ h}^{-1}$ , above which the input signal is very attenuated, distorted and incoherent (Fig. 9). The mean delay calculated by Eq. (20) in the low frequencies is 2 h. For the ZJS spring, variation of the

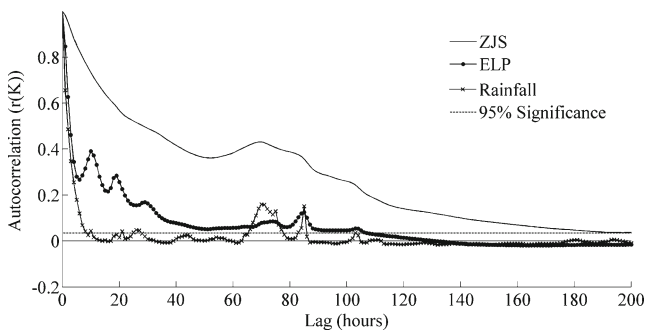


**Fig. 10** Autocorrelation functions of rainfall and flow discharges for ZJS and ELP springs

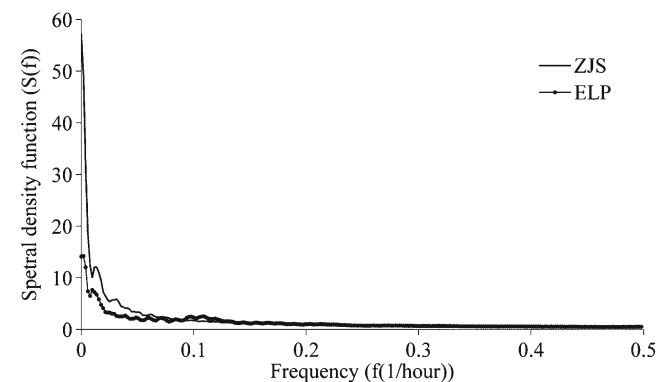


**Fig. 11** Spectral density functions of flow discharges for ZJS and ELP springs

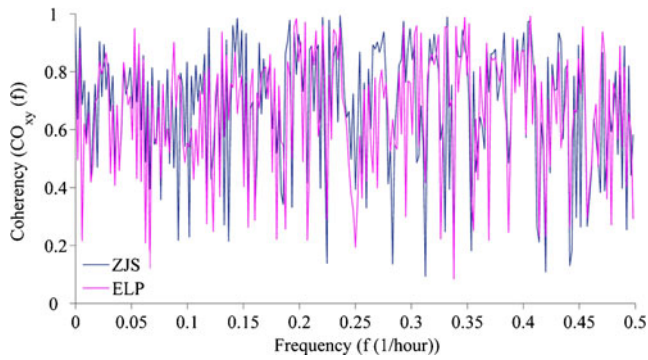


**Fig. 12** Coherency functions of flow discharges for ZJS and ELP springs

phase function is consistent and the mean delay at low frequencies cannot be distinguished.

The cross-correlation  $r_{xy}(k)$  and the cross-amplitude function  $|S_{xy}(f)|$  are associated with the duration of the impulse response function (Padilla and Pulido-Bosch 1995; Larocque et al. 1998). They indicate the filtering of the periodic components of the rainfall data. The degree of transformation of the input signal depends on the structure of the karst system and represents some kind of a filter which transforms the input signal. A poorly developed karst system with high storage capacity can be considered as an inertial filter, which attenuates most of the short term (high frequencies) input signals. The non-inertial character of the aquifer informs about the well-developed stage of its karstification as well as the lack of regulating underground reserves of some importance.

The time lag of the thick epikarst zone of ZJS is longer than that of the thin epikarst zone of ELP, indicating that response of the peak flow of ELP spring to a rainfall event is more rapid than that of ZJS spring. The results also indicate a predominant role of the quickflow component and small regulation effect of the epikarst zone on ELP spring flow, and a relatively weak role of the quickflow component and large regulation effect of the epikarst zone on ZJS spring flow.

#### Long term response of spring hydrograph to rainfall

Time lag information in Table 2 shows that long term response of the spring hydrograph to rainfall can be

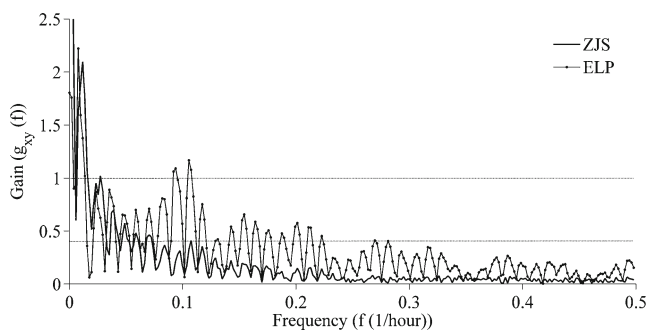


**Fig. 13** Gain functions of flow discharges for ZJS and ELP springs

represented by memory effect, regulation time and periodic variations of autocorrelation function  $r(k)$  and cross-correlation function  $r_{xy}(k)$ , respectively. The memory effect is computed on the basis of decorrelation lag time, defined as the time at which the autocorrelation function attains a predetermined value (Mangin 1984). Figure 10 illustrates the autocorrelation functions,  $r(k)$ , calculated by Eq. (1) for the flow discharges at both springs. The memory effect determined by Eq. (4) is 0.034 at the 95 % significance level. The  $r(k)$  value of 0.034 corresponds to the time delay of 198 h for ZJS spring and 107 h for ELP spring.

The regulation time  $T_{reg}$  is a way of comparing systems and can be thought of as the time at which half of the system signal has been exhausted or as a passing band in signal treatment (Larocque et al. 1998). From the spectral density function  $S(f)$  in Fig. 11, the regulation time  $T_{reg}$  computed by Eq. (7) is 210 and 143 h for ZJS and ELP springs, respectively. The computed memory effect implies that decrease of groundwater flow from ZJS spring is slower than that of ELP spring because the storage capacity for the thick epikarst zone of ZJS is much larger than that of the thin epikarst zone of ELP.

The shape of the correlogram and the derived memory effect depend not only on the state of maturity of the karst system but also the frequency and distribution of the precipitation events (Kovács and Sauter 2007). For the same karst aquifer, the higher the frequency of the flood, the faster the fall off of the correlogram (Eisenlohr et al. 1997; Kovács and Sauter 2007). For both ZJS and ELP springs, a series of peaks in the autocorrelation function ( $r(k)$  in Fig. 10) and cross-correlation function ( $r_{xy}(k)$  in Fig. 7) were observed after the first peak, indicating that periodic components of the rainfall and several flow components within an epikarst zone are detected. The coherence function ( $CO_{xy}(f)$  in Fig. 12) also proves that the correlation between the periodic variables is strong. It shows that correlation coefficients between the input and output variables for ZJS and ELP springs are 0.64 and 0.65, respectively.

Figure 10 shows that there is a notable periodic component ( $r(k) > 0.034$ ) for a 70-h period between two discrete components for ZJS and a 10-h period among the notable three discrete components for ELP. Figure 7 shows a notable periodic component for a 71-h period between two primary discrete components for both ZJS and ELP springs, and a 10-h period between the first two discrete components in ELP spring. The notable periodic component of 71 h corresponds to the notable periodic component of 71 h for the rainfall series in the study catchment. These analyses indicate that the time intervals between the periodic components of the flow discharge for ELP are generally much shorter than those of ZJS.

#### Intermediate term response of spring hydrograph to rainfall

Figures 7 and 10 show that correlation functions decrease rather quickly during the initial period. The durations of

**Table 2** Hydrological parameters in Chengqi watershed. *ND* not distinguishable

Effect	Time lag for ZJS (hours)	Time lag for ELP (hours)	Indicator	Method
Short-term response	2	1	Time of correlogram peak $d = \frac{\theta_{xy}(f)}{2\pi f}$	Cross-correlation, $r_{xy}(k)$ Phase function, $\theta_{xy}(f)$
	ND	2		
Intermediate-term response	<5	<3	$ S_{xy}(f) $ tends to be zero	Cross-amplitude function $ S_{xy}(f) $
	23	6	Initially sharp decline of $r(k)$	Auto-correlation, $r(k)$
	24	9	Initially sharp decline of $r_{xy}(k)$	Cross-correlation, $r_{xy}(k)$
Long-term response	198	107	Memory effect $r_k=0.034$	Auto-correlation, $r(k)$
	70	10	Length between periodic components	Auto-correlation, $r(k)$
	71	10	Length between periodic components	Cross-correlation, $r_{xy}(k)$
	210	143	Regulation time $T_{reg} = \frac{S(f=0)}{2}$	Spectral density function, $S(f)$
Duration of quick flow	9	4	$g_{xy}(f) > 1$	Gain functions, $g_{xy}(f)$
Duration of slow flow	181	71	$g_{xy}(f) < 0.4$	Gain functions, $g_{xy}(f)$

the fastest decline in slope of the autocorrelation function  $r(k)$  and the cross-correlation function  $r_{xy}(k)$  in Table 2 are between the time lags of the short-term and long-term responses of the spring hydrograph to rainfall. The fast or slow decline of the autocorrelation function reflects the state of maturity of the karst system. The faster the drop in the auto-correlation function, the weaker the groundwater flow reserves in an aquifer and, hence, an active karst network. Inversely, a strong memory effect will convert a strong discharge into a major stocking of the groundwater flow reserves of an aquifer (Eisenlohr et al. 1997).

The initially fastest decline of  $r_{xy}(k)$  in Fig. 7 lasts 24 and 9 h for ZJS and ELP, respectively. The initially sharp descent of  $r(k)$  in Fig 10 endures about 23 h for ZJS spring and 6 h for ELP spring. The results reflect the length of the impulse response of flow discharge in the primary fracture system to the input signal. Declines of spring flow discharge in a shorter period from ELP and a relatively longer period from ZJS indicate that the proportion of large fractures in the thin epikarst zone of ELP is much greater than that in the thick epikarst zone of ZJS.

#### Duration of baseflow and quickflow

Figure 13 shows existence of the non-linear processes which govern the hydrogeological functioning of a karst aquifer. These non-linear processes are mainly due to two different modes of transfer for quick flows (due to the

presence of large fractures) and slow flows released from storage. In a karst aquifer, the output signal is amplified when the spring flow derives from the release of storage water. The gain function in Fig. 13,  $g_{xy}(f)$ , expresses an amplification ( $>1$ ) or an attenuation ( $<1$ ) of the output signal in comparison with the input signal. In a karstic environment, this phenomenon can be related to the storage of water during the high water period and the release of water during the dry period. During rainfall periods, the inflow from rainfall was frequent enough to cause a dominant role of groundwater flow through larger open fissures and fractures or karst conduits (quick flow), and the fast-draining pathways have high flow amplitudes. During dry periods, the frequent flow changes in these pathways were dampened due to the influence of the surrounding matrix (Kovács and Sauter 2007) and baseflow became a dominate role of groundwater flow.

The gain functions ( $g_{xy}(f)$  in Fig. 13) of ZJS and ELP springs show powerful filtering and attenuation effects, where the input signals are hardly changed at low frequencies. According to the analysis by Padilla and Pulido-Bosch (1995), the  $g_{xy}(f)$  value of 1 coincides with the duration of the impulse response of the aquifer's baseflow component, and the value of 0.4 corresponds with duration of the quickflow component. Between these two ranges, it could be considered as intermediate flow. For ZJS spring, durations of quick and slow flow components are 9 and 181 h (corresponding to  $f=0.11$  and  $0.0055 \text{ h}^{-1}$ ), respectively. For ELP

**Table 3** Hydrological parameters for two representative karst systems of Greece (Panagopoulos and Lambrakis 2006)

Effect	Time lag for Trifilia (days)	Time lag for Almyros (days)	Indicator	Method
Short-term response	66	4	Peak of correlogram $d = \frac{\theta_{xy}(f)}{2\pi f}$	Cross-correlation, $r_{xy}(k)$ Phase function, $\theta_{xy}(f)$
	–	4.5		
Intermediate-term response	25	5	$ S_{xy}(f) $ tends to zero	Cross-amplitude function $ S_{xy}(f) $
	–	6	Initially sharp decline of $r(k)$	Auto-correlation, $r(k)$
Long-term response	83	55	Memory effect $r_k=0.2$	Auto-correlation, $r(k)$
	200 <sup>a</sup>	83 <sup>a</sup>	Regulation time $T_{reg} = \frac{S(f=0)}{2}$	Spectral density function, $S(f)$
Duration of quick flow	34	4.5	$g_{xy}(f) > 1$	Gain functions, $g_{xy}(f)$
Duration of slow flow	136	22	$g_{xy}(f) < 0.4$	Gain functions, $g_{xy}(f)$

<sup>a</sup> Indicates that values are estimated from figures of Panagopoulos and Lambrakis (2006). – represents data unavailable

**Table 4** Hydrological parameters for the karstic systems in the south-east of Spain and the French Pyrenees (Padilla and Pulido-Bosch 1995). *ND* not distinguishable

Effect	Time lag for Aliou (days)	Time lag for Baget (days)	Time lag for Simat (days)	Time lag for E1 Torcal (days)	Indicator	Method
Short-term response	<1 0.5	<1 0.5	2 1	12–35 20	Peak of correlogram $d = \frac{\theta_{xy}(f)}{2\pi f}$	Cross-correlation, $r_{xy}(k)$ Phase function, $\theta_{xy}(f)$
Intermediate-term response	<3 5 <sup>a</sup>	<3 5 <sup>a</sup>	5–7 10 <sup>a</sup>	20 ND	$ S_{xy}(f) $ tends to zero Initially sharp decline of $r_{xy}(k)$	Cross-amplitude function $ S_{xy}(f) $ Cross-correlation, $r_{xy}(k)$
Long-term response	12	20	60–80	>100	Length between periodic components	Cross-correlation, $r_{xy}(k)$
Duration of quick flow	3	5	9	38	$g_{xy}(f) > 1$	Gain functions, $g_{xy}(f)$
Duration of slow flow	24	24	38	63	$g_{xy}(f) < 0.4$	Gain functions, $g_{xy}(f)$

<sup>a</sup> Indicates that values are estimated from figures of Padilla and Pulido-Bosch (1995)

spring, durations of quick and slow flow components are 4 and 71 h (corresponding to  $f=0.281$ , and  $0.014 \text{ h}^{-1}$ ), respectively. The results indicate that the time lag of response of quick flow component to rainfall is the same for ELP and ZJS springs, but the time lag for the slow flow component in the thicker epikarst zone of ZJS is much longer than that of the thinner epikarst zone of ELP.

## Conclusions and discussion

Time-series analysis of hourly spring flow discharge and rainfall was carried out for two hillslopes with different thicknesses of epikarst zone. The comparison of the analysis results enabled characterization of the transformations between input (rainfall) and output (spring discharge) for the hillslope epikarst zones. Length of the time lag of spring flow discharge and its relation to rainfall are derived from correlation and spectral density functions in the karst area of southwest China. They are used as indicators to classify short, intermediate and long-term responses of the spring hydrograph to rainfall. Validation of this classification using the indicators in other karst areas is discussed in the following.

Tables 3 and 4 list the results by Panagopoulos and Lambrakis (2006) and Padilla and Pulido-Bosch (1995), respectively, using time-series analysis in karst watersheds. Table 3 shows that values of the time-lag of two representative karst systems of Greece (Trifilia in Peloponnesus and Almyros in Crete) computed by auto- and cross-correlation and spectral density function can be grouped into three types according to the classifying methods in this study. The slightly karstified Trifilia karst system with a large storage capacity has a longer time lag than the Almyros karst system with the developed karst network. Table 4 is the analysis results by Padilla and Pulido-Bosch (1995) for the four karstic systems, two situated in the south-east of Spain (E1 Torcal and Simat) and two in the French Pyrenees (Aliou and Baget) using cross-correlation and spectral density function. The results also prove that the time lags can be grouped into the three

types. It was found that the initially sharp decline of the cross-correlogram of rainfall–discharge at E1 Torcal does not exist because the quickflow is practically absent.

A noteworthy conclusion of this study is that the thickness of epikarst has an important influence on the hydrological processes in the epikarst zone. The lengths of the time lag for short-, intermediate- and long-term responses and durations of slow and quick flow components for the thick epikarst zone with large storage capacity are much longer than those in the thin epikarst zone with small storage capacity. Field investigation demonstrates that the proportion of the large fractures in the shallow epikarst zone is much greater than that in the deep epikarst zone. Porosity reduces significantly from the ground surface to the epikarst bed. The thick epikarst zone contains more slow-flow components and thus presents a longer delay response of the hydrograph to rainfall.

The classifying indicators reflect effects of karst zone storage capacity and rainfall characteristics on flow discharge. The short-term response of spring discharge to rainfall is quantified by length of the time lag between the storm pulse and the peak in the discharge hydrograph, primarily reflecting quick flow response during the flood period in larger open fissures and fractures or karst conduits. The intermediate-term response is quantified by the length of the impulse response of the hydrograph to overall rainfall events, reflecting the responses of quick flow and the portion of baseflow through the primary fracture system of larger open fissures and fractures or karst conduits. Long-term memory effect identifies characteristics of a long-term discharge time series, particularly cyclic variations of flow discharge and rainfall series, persistency and memory for the low groundwater flow rate in the small fractures of the karst system.

**Acknowledgments** This research was supported by the National Natural Scientific Foundation of China Nos. 40930635, 41101018, 51079038, and 51190090. We thank the editor and three anonymous reviewers for their constructive comments on the earlier manuscript, which lead to an improvement of the report.

## References

- Al-fares W, Bakalowicz M, Gue'rine R, Dukhan M (2002) Analysis of the karst aquifer structure of the Lamalou area (He'rault, France) with ground penetrating radar. *J Appl Geophys* 51(2-4):97-106
- Amraoui F, Razack M, Bouchaou L (2003) Turbidity dynamics in karstic systems: example of Ribaa and Bittit springs in the Middle Atlas (Morocco). *Hydrol Sci J* 48(6):971-984
- Benavente J, Pulido-Bosch A, Mangin A (1985) Application of correlation and spectral procedures to the study of the discharge in a karstic system (eastern Spain). In: *Karst Water Resources, Proceedings, Ankara-Antalya, Turkey, July 1985*, pp 67-75
- Beres M, Haeni FP (1991) Application of ground penetrating radar methods in hydrogeologic studies. *Ground Water* 29(3):375-386
- Beres M, Luetscher M, Olivier R (2001) Integration of ground penetrating radar and microgravimetric methods to map shallow caves. *J Appl Geophys* 46:249-262
- Bonacci O (1993) Karst springs hydrographs as indicators of karst aquifers. *Hydrol Sci J* 38(1):51-62
- Box GEP, Jenkins GM, Reinsel GC (1994) *Time series analysis: forecasting and control*, 3rd edn. Prentice Hall, Englewood Cliffs, NJ
- Chen X, Chen C, Hao Q, Zhang Z, Shi P (2008) Simulation of rainfall underground outflow responses of a karstic watershed in southwestern China with an artificial neural network. *Water Sci Eng* 1(2):1-9
- Eisenlohr L, Kiraly L, Bouzelboudjen M, Rossier Y (1997) Numerical simulation as a tool for checking the interpretation of karst spring hydrographs. *J Hydrol* 193(1-4):306-315
- Ford DC, Williams PW (1989) *Karst geomorphology and hydrology*. Unwin Hyman, London
- Ford DC, Williams PW (2007) *Karst hydrogeology and geomorphology*. Wiley, Chichester, UK, 561 pp
- Gand KC, McMahon TA, Finlayson BL (1991) Analysis of periodicity in streamflow and rainfall data by Cowell's indices. *J Hydrol* 123:105-118
- Jenkins GM, Watts DG (1968) *Spectral analysis and its applications*. Holden Day, San Francisco, 525 pp
- Kovács A, Sauter M (2007) Modelling karst hydrodynamics. In: Goldscheider N, Drew D (eds) *Methods in karst hydrogeology*, vol 26. International Contribution to Hydrogeology, Heise, Hanover, Germany, pp 201-220
- Lambrakis N, Andreou AS, Polydoropoulos P, Georgopoulos E, Bountis T (2000) Non-linear analysis and forecasting of a brackish karstic spring. *Water Resour Res* 36(4):875-884
- Larocque M, Mangin A, Razack M, Banton O (1998) Contribution of correlation and spectral analyses to the regional study of a large karst aquifer (Charente, France). *J Hydrol* 205:217-231
- Lee JY, Lee KK (2000) Use of hydrologic time series data for identification of recharge mechanism in a fractured bedrock aquifer system. *J Hydrol* 229:190-201
- Maloszewski P, Stichler W, Zuber A, Rank D (2002) Identifying the flow systems in a karstic-fissured-porous aquifer, Scheealpe, Austria, by modelling of environmental <sup>18</sup>O and <sup>3</sup>H isotopes. *J Hydrol* 256:48-59
- Mangin A (1975) Contribution a l'etude hydrodynamique des aquiferes karstiques [Contribution to the hydrodynamic study of karst aquifers]. *Ann Spéioliol* 29:283-332
- Mangin A (1984) Pour une meilleure connaissance des systemes hydrologiques a partir des analyses corre'latoire et spectrale [For a better understanding of hydrological systems from correlation and spectral analysis]. *J Hydrol* 67:25-43
- McMechan GA, Loucks RG, Zeng X, Mescher P (1998) Ground penetrating radar imaging of a collapsed paleocave system in the Ellenburger dolomite, central Texas. *J Appl Geophys* 39:1-10
- Padilla A, Pulido-Bosch A (1995) Study of hydrographs of karstic aquifers by means of correlation and cross-spectral analysis. *J Hydrol* 168:73-89
- Panagopoulos G, Lambrakis N (2006) The contribution of time series analysis to the study of the hydrodynamic characteristics of the karst systems: application on two typical karst aquifers of Greece (Trifilia, Almyros Crete). *J Hydrol* 329(3-4):368-376
- Perrin J (2003) A conceptual model of flow and transport in a karst aquifer based on spatial and temporal variations of natural tracers. PhD Thesis, University of Neuchâtel, Switzerland
- Trček B (2007) How can the epikarst zone influence the karst aquifer hydraulic behaviour? *Environ Geol* 51(5):761-765
- Williams PW (1983) The role of the subcutaneous zone in karst hydrology. *J Hydrol* 61(1-3):45-67
- Williams PW (2008) The role of the epikarst in karst and cave hydrogeology: a review. *Int J Speleol* 37(1):1-10
- Zhang ZC, Chen X, Cheng QB, Peng T, Zhang YF, Ji ZH (2011) Study of hydrogeology of epikarst in karst mountain: a case study of Chenqi catchment (in Chinese). *Earth Environ* 39(1):19-25